Chemical Science

ROYAL SOCIETY OF CHEMISTRY

EDGE ARTICLE

View Article Online
View Journal | View Issue

Cite this: *Chem. Sci.*, 2025, **16**, 13333

All publication charges for this article have been paid for by the Royal Society of Chemistry

Received 10th October 2024
Accepted 10th April 2025

DOI: 10.1039/d4sc06894g

rsc.li/chemical-science

Reversible addition of ethene to gallium(I) monomers and dimers†

Ryan J. Schwamm,‡ Malavika A. Bhide,‡ Gary S. Nichol and Michael J. Cowley *

Reversible interactions of organic substrates with transition metal compounds are a hallmark of their chemistry and its catalytic applications, but remain uncommon for low-valent p-block compounds. We report here the preparation of amidophosphine-supported gallium(I) compounds that exhibit equilibria between monomeric gallylene and dimeric digallene (Ga=Ga) states. The monomer–dimer equilibrium is controlled by the steric and electronic properties of the phosphine donor in the ligand employed. Regardless of their preference for monomeric or dimeric state, reactions of the Ga(I) systems with $B(C_6F_5)_3$ affords monomeric gallylene adducts, whilst reactions with ethene produce 1,2-digallacyclobutanes *via* formal [2 + 2] cycloadditions. These ethene additions are reversible, with the digallacyclobutanes releasing ethene upon heating or treatment with Lewis acids to regenerate the gallium(I) species.

Introduction

Reversible reactivity is a hallmark of transition-metal chemistry, in which the combination of reversible steps including ligand exchange, oxidative addition, and reductive elimination enables powerful catalytic processes. In main group chemistry, the widespread capability of low-oxidation state p-block compounds to engage in somewhat similar reactivity, particularly oxidative additions, has emerged relatively recently.[1,2] It is still unclear how (and even if) this reactivity may serve as the basis of a general 'redox-cycle catalysis' at p-block element centres, even considering recent ground-breaking advances in redox-catalytic cycles at group 15 centres.[3–6] Thus it remains a general challenge to engineer p-block systems in which oxidative addition reactions are readily reversible.[7]

Reactions of main group species with unsaturated organic molecules such as alkenes and alkynes are relatively common, but normally irreversible.[1,8–10] A few examples of reversible reactions have been reported. In group 14 chemistry, Kato reported reversible ethene binding at an amidophosphine supported Si(II) centre.[11] Previous to that, Power reported reversible ethene binding by tin alkyne analogues,[12] and more recently Tokitoh extended this reversibility to di germynes.[13] In group 13 chemistry, the group of Crimmin has shown that the Al(I) monomer NacNacAl(I) can reversibly bind alkenes.[14] Power reported terphenyl Ga(I) systems – which may adopt monomeric or dimeric structures in solution[15,16] – that reversibly react with polyolefins.[17] Dicationic digallenes also reversibly bind alkenes.[18] Recently reported base-stabilised dialumenes react with alkenes and alkynes,[19–21] in some cases dissociating to monomeric Al(I) species before doing so,[19] but these reactions are not reversible. The related gallium analogues (base-stabilised digallenes) remain comparatively underexplored, and no reactivity with olefins is reported for them.[22] The origins of the reversibility (or otherwise) in the reactions of Al(I) and Ga(I) with olefins remain unclear, as does its connection with the nuclearity of the reactive species.

Ga(I) chemistry is structurally rich, with compounds ranging from larger clusters to monomeric species.[15–17,23–26] Dimeric systems can be divided into two classes: (i) weakly associated systems with low Ga–Ga bond order and (ii) 'true' dimers with Ga–Ga bond orders >1. Systems like Power's terphenyl Ga(I) series **I** or Stasch's $[Ph_2P(NDipp)_2Ga]_2$ (ref. 27) exhibit weak interactions characterised by long Ga–Ga distances and significant *trans*-bending. The terphenyl Ga(I) systems **I** are almost wholly monomeric in solution.[15,16,23] Nevertheless, indirect evidence implicates formation of transient Ga=Ga dimers in reactions with olefins.[17] In the related $Ar^{iPr8}Al$(I) system, which is observed to exist as both monomers and/or Al=Al bonded dimers, the mechanism of reactions with ethene are complex.[28]

Despite early reports of supported $[R_4Ga_2]^{2-}$ and $[R_4Ga_2]^{\bullet}$ species featuring Ga–Ga bond orders ≥1 over 20 years ago,[29–31] the first well-defined example of a neutral closed-shell digallene **II** was only recently presented.[22] The NHC-coordinated digallene **II** is the gallium analogue of Inoue's landmark dialumene, **III**.[20] The strong donor ligands of **II** imbue it with a strong Ga=Ga bond and short Ga–Ga distance ((2.341(3) Å) *vs. e.g.* 2.627(1) Å for **I**). No reactivity of **II** with small molecules has been reported.

School of Chemistry, The University of Edinburgh, Joseph Black Building, David Brewster Road, Edinburgh EH9 3FJ, UK. E-mail: michael.cowley@ed.ac.uk

† Electronic supplementary information (ESI) available. CCDC 2384332–2384338, 2433601, and 2433602. For ESI and crystallographic data in CIF or other electronic format see DOI: https://doi.org/10.1039/d4sc06894g

‡ These authors contributed equally to this work.

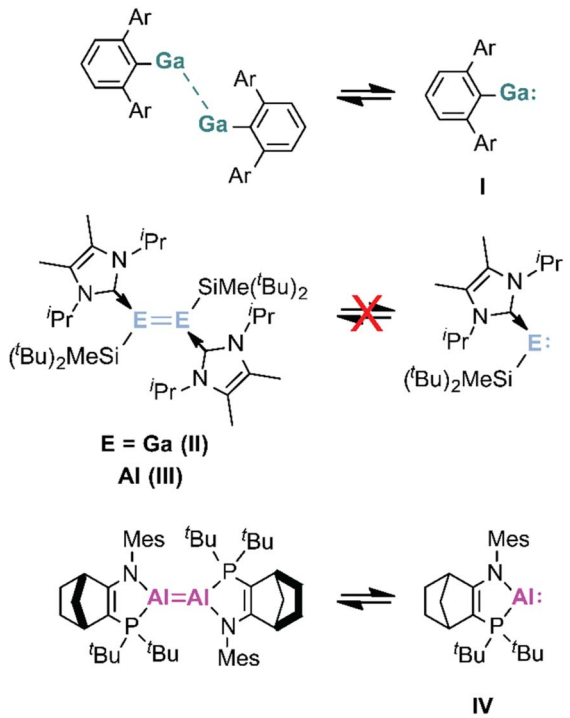

Fig. 1 Structures of low valent Al and Ga species. Ar = 2,6-$Dipp_2C_6H_3$, Mes = $C_6H_2Me_3$.

Krossing and co-workers have investigated related dicationic digallene systems that react with a range of small molecules.[31–33] In chemistry related to that of dialumene **III**, we recently reported the synthesis of the *trans*-bent base-coordinated dialumene **IV**, supported by an amidophosphine ligand system.[19]

The amidophosphine ligands of **IV** are conveniently prepared, provide a useful ^{31}P NMR 'handle' for characterisation and mechanistic insight, and in principle are readily modified at the phosphorus centre to vary both electronic and steric properties. We were curious whether such amidophosphine ligands could shed light on Ga(I) chemistry and provide improved control or understanding of speciation within it.

Here, we show that the amidophosphine ligand used to support dialumene **IV** may be transferred successfully to Ga(I) chemistry, in the process developing a high-yielding preparative route to Ga(I) systems. By altering the size of the substituents on the phosphine, we demonstrate the ability to tune Ga(I) systems to favour monomeric (gallylene) or dimeric (digallene) states. Regardless of their preference for monomer/dimer, the amidophosphine Ga(I) species we report react with ethene to form digallacyclobutanes – products containing two Ga centres. Remarkably, these digallacyclobutanes reversibly release ethene upon heating or by treatment with Lewis acids (Fig. 1).

Results and discussion

A digallene

For the preparation of digallene **1**, the gallium analogue of dialumene **IV**, we envisaged a simple salt metathesis route with a gallium subhalide (*e.g.* "GaI"). However, with the lithiated amidophosphine ligand precursor $L^{Mes/tBu}Li(OEt_2)$ (see ESI†), these reactions led only to intractable mixtures. The substitution of Cp* ligands in Cp*Ga or $(Cp^*Al)_4$ with metalated ligands is emerging as a useful route to neutral or anionic Ga(I) or Al(I) compounds.[34,35] We decided to trial this strategy for our amidophosphine ligands.

The reaction of Cp*Ga with the lithiated amidophosphine ligand $L^{Mes/tBu}Li(OEt_2)$ in toluene at 80 °C (Fig. 2) generated a red solution. $^{31}P\{^1H\}$ NMR spectroscopy revealed the formation of a new phosphorus-containing species with a broad resonance at δ 26.0 and, after three hours, copious quantities of orange precipitate – the digallene $L^{Mes/tBu}Ga = GaL^{Mes/tBu}$ (**1**) – had formed. Following recrystallisation, digallene **1** was obtained as red crystals in 74% yield.

Digallene **1** is a Ga(I) dimer in the solid-state. The structure of **1** (Fig. 2), determined by X-ray diffraction, very closely resembles that of dialumene **IV**, including in the 2-site disorder of the symmetry-related Ga centres (70/30% occupancy). The disorder arises from the heavily *trans*-bent Ga=Ga bond (*trans*-bend angle θ = 55.6/57.6°), which displays Ga1–Ga1′ distances of 2.480(1) and 2.468(3) Å. The phosphorus substituents are

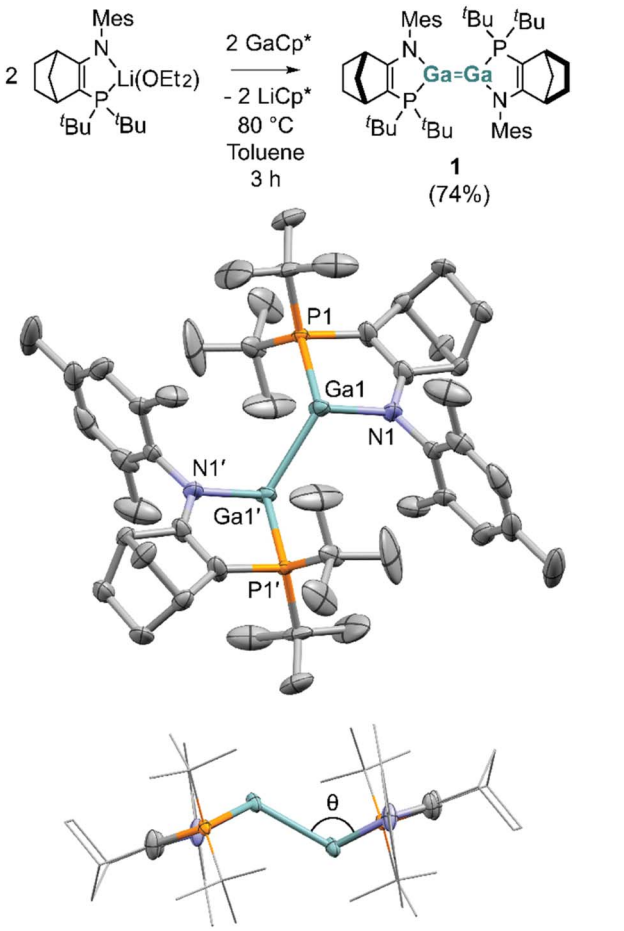

Fig. 2 Synthesis of digallene **1**. X-ray structure of **1** (H atoms omitted for clarity). Thermal ellipsoids at 50% probability. Selected bond distances (Å) and angles (°): Ga1–Ga1′ 2.480(1), Ga1–N1 2.002(3), Ga1–P1 2.513(6), N1–Ga1–P1 82.55(15), θ = 55.6.

trans to one another across the Ga=Ga bond, meaning the digallene exists in *E*-configuration.

Dialumene **IV**, the aluminium analogue of digallene **1**, features a notably longer Al=Al bond than its NHC/silyl substituted counterpart dialumene **III**.[20] The same pattern is observed in the gallium analogues: the Ga–Ga distance in **1** is longer than in Wang's NHC/silyl substituted digallene **II** (2.480(1)/2.468(3) Å *vs.* 2.341(3) Å).[22]

Density functional theory (DFT) calculations (BP86-D3/def2svp) on digallene **1** reveal the presence of a Ga=Ga π-bonding interaction (Fig. S4†). As in dialumene **IV**, the HOMO of **1** has substantial Ga–Ga π-bonding character (Fig. S4†). Consistent with this, the calculated Wiberg bond index (WBI) for the Ga=Ga bond is 1.24, which supports the conclusion of a degree of multiple bonding character. Compared to the same measure in Wang's NHC/silyl substituted digallene **II**, however, the WBI in **1** is much lower (1.71 *vs.* 1.24).[22] This is consistent with the ~0.13 Å shorter Ga–Ga bond distance in **II**. In fact, the Ga1–Ga1′ distance in digallene **1** falls approximately midway between that in **II** and that for Power's weakly associated terphenyl Ga(I) species **I** (2.627(1) Å),[24] which dissociates in solution. With the stretched Ga=Ga distance and low calculated bond-order in **1**, we became curious about its solution behaviour.

Digallene **1** exists in solution as a mixture of monomers and dimers. Like its aluminium analogue **IV**,[19] the *E* isomer of digallene **1** has three possible diastereomers, **1A**, **1B** and **1C**. **1A** and **1B** are *meso*-compounds, and each have equivalent phosphorus centres; they both should thus have one phosphorus chemical shift. In contrast, the two phosphorus centres in **1C** are chemically inequivalent, and so this compound should give rise to two ^{31}P NMR signals. At 300 K, the ^{31}P{^{1}H} NMR spectrum of digallene **1** reveals a single broad resonance at δ 26.0, indicating that all three diastereomers **1A–C** are interconverting rapidly on the NMR timescale.

Upon cooling, the exchange of diastereomers slows and the single broad ^{31}P resonance becomes further resolved (Fig. 3a).

The dynamic processes involved in the exchange of diastereomers **1A–C** are more clearly apparent in the ^{1}H NMR spectrum (Fig. 3a). At room temperature, one signal at δ 3.03 for the NCC*H* bridgehead proton of all three diastereomers is observed. On cooling to 233 K, the resonance splits into two new singlets, at δ 3.00 and δ 3.05. We assign one of these signals to diastereomers **1A** and **1B**, which are interconverting by an

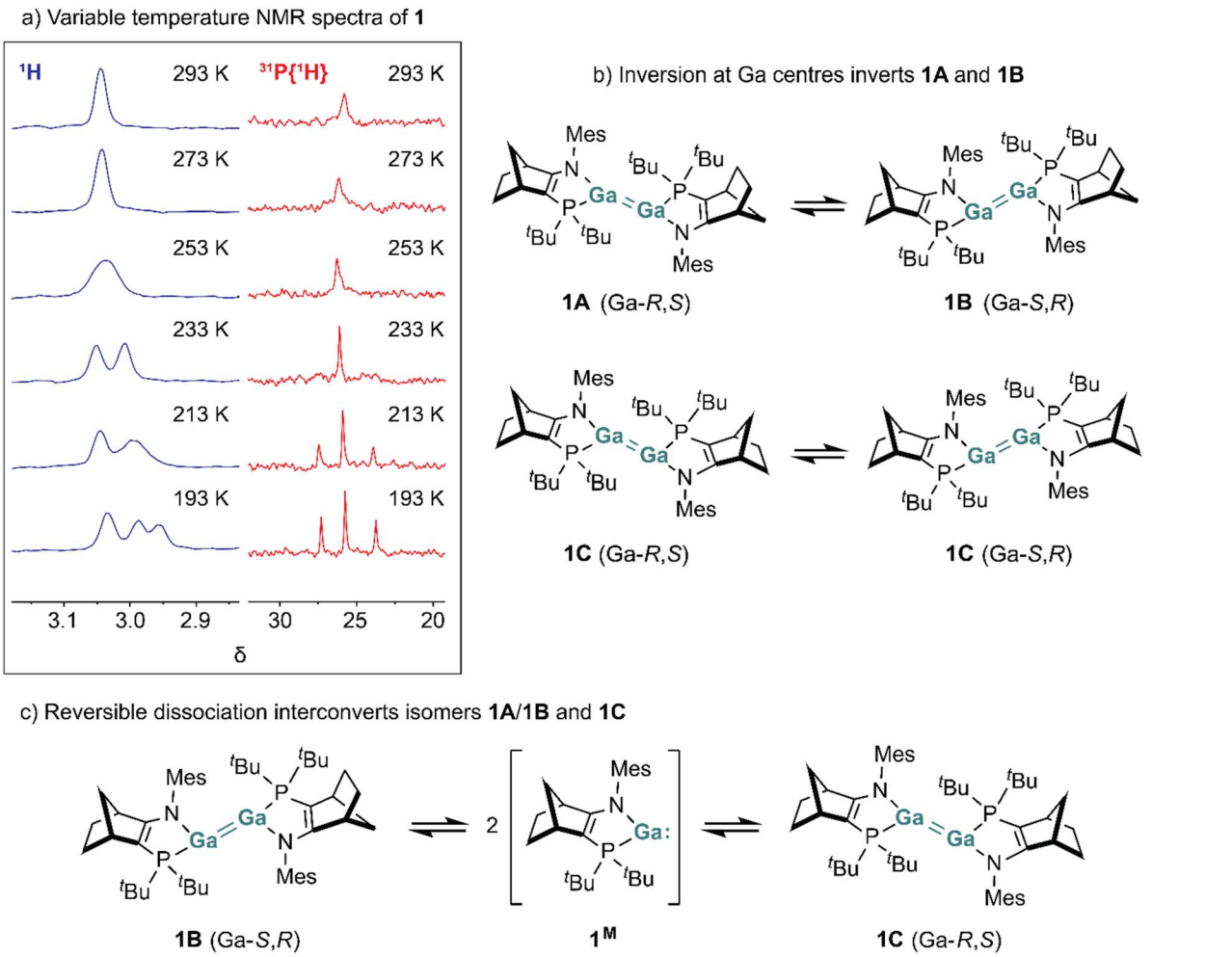

Fig. 3 (a) ^{1}H and ^{31}P{^{1}H} VT NMR spectra of **1**. (b) Ga inversion mechanism between **1A** and **1B**, and enantiomers of **1C**. (c) Dissociation pathway for interconversion of **1A**/**1B** and **1C**.

intramolecular process that simultaneously inverts the stereochemistry at both Ga centres (Fig. 3b); a related "*trans*-flip" process is operative in the dialumene **IV**.[19] The trans-flip exchanges the two inequivalent bridgehead CH environments of **1C**, thus explaining the appearance of just one resonance for this diastereomer. On cooling still further, to 193 K, the signal observed at δ 3.00 at 233 K itself resolves into two new singlets at δ 2.99 and δ 2.95 due to a slowing of the *trans*-flip process between **1A**/**1B** or for **1C**. It is not possible to unequivocally assign whether it is exchange between **1A**/**1B** or between CH environments in **1C** which becomes slow at 193 K.

For the digallene **1** in solution at room temperature, the observation of just one signal for the NCC*H* bridgehead proton indicates all three diastereomers **1A–C** are rapidly exchanging. Since the *trans*-flip process cannot interconvert **1A**/**1B** with **1C**, this exchange can only be through reversible dissociation of the digallene into monomers (Fig. 3c).

Although the NMR spectroscopic behaviour of digallene **1** can only be explained by invoking its reversible dissociation into monomers, the compound nevertheless exists predominantly as a dimer in solution. The UV/vis spectrum of **1** in Et_2O reveals an intense absorption at λ_{max} = 501 nm (ε = 9847 mol L^{-1} cm^{-1}) (Fig. S54†). TD-DFT calculations (BP86-D3/Def2SVP) on **1** allowed us to assign the absorption to an excitation with substantial contributions from Ga=Ga π to π^*-type transition (HOMO → LUMO (Fig. S4†)), as well as a smaller contribution from a ligand-based orbital (HOMO−2 → LUMO). The spectroscopic measurements reveal that **1** has a marginally narrower HOMO–LUMO gap than the reported digallene **II** (λ_{max} = 521 nm).[22]

A gallylene

In transition metal chemistry, ready steric and electronic tuning of phosphine ligands allows powerful control over the properties and reactivity of transition-metal complexes.[36] We were curious whether the same effects might translate to low-valent p-block chemistry.

We thus prepared $HL^{Mes/Mes}$, an analogue of the amidophosphine ligand of **1** in which the P^tBu_2 donor has been replaced with the diaryl phosphine fragment $PMes_2$. We expected the $PMes_2$ fragment should be both less electron-donating and more sterically hindered than P^tBu_2.

The lithium salt of the ligand, $L^{Mes/Mes}Li(OEt_2)$, was readily obtained by treatment of $HL^{Mes/Mes}$ with *n*-butyl lithium (see ESI†).

Dropwise addition of a solution of $L^{Mes/Mes}Li(OEt_2)$ to Cp*Ga in toluene initially formed a yellow solution, which became dark orange and deposited a colourless precipitate (Cp*Li) after it was heated to 80 °C for 3 hours. $^{31}P\{^1H\}$ NMR spectroscopy of the crude reaction mixture revealed the formation of a new compound exhibiting a singlet at δ −38.7. The new compound was isolated by crystallisation from pentane as a yellow solid in 45% yield.

X-ray diffraction reveals the yellow crystalline material obtained from pentane to be the monomeric gallylene species $L^{Mes/Mes}Ga$ (**2**), which features a two-coordinate gallium centre

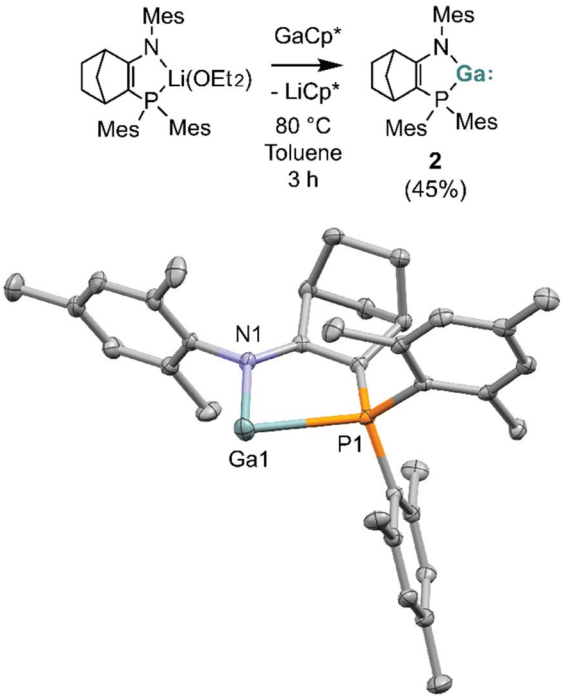

Fig. 4 Synthesis of gallylene **2**. X-ray structure of **2** (H atoms omitted for clarity). Thermal ellipsoids at 50% probability. Selected bond distances (Å) and angles (°): Ga1–N1 1.962(2), Ga1–P1 2.7093(5), N1–Ga1–P1 78.92(5).

(Fig. 4). The Ga–P distance, at 2.7093(5) Å, is substantially (~0.2 Å) elongated compared to that in digallene **1** (2.47–2.51 Å). Concurrently, the bite angle P1–Ga1–N1 in gallylene **2** is narrowed compared to that in **1** (78.92(5)° *vs.* 82.66(15)°). The increased Ga–P distance in **2** is consistent with the greater steric bulk and lower donating ability of the $PMes_2$ (*vs.* P^tBu_2 in digallene **1**).

Consistent with the monomeric structure observed for gallylene **2** in the solid state, NMR spectroscopy reveals no evidence for formation a dimeric digallene ($[\mathbf{2}]_2$) in toluene solutions. Thus, the room temperature $^{31}P\{^1H\}$ spectrum of gallylene **2** showed a single broad resonance at δ −37.8. The formation of the putative digallene $[\mathbf{2}]_2$ would be expected to be revealed by the presence of ^{31}P resonances for multiple diastereomers (in the absence of any reversible dissociation). Even on cooling a solution of gallylene **2** in d_8-toluene to 193 K, the signal at δ −37.8 remained a singlet. If the dimer $[\mathbf{2}]_2$ forms under such conditions it must therefore be in low concentrations, or remain in equilibrium with the monomeric gallylene **2**.

The room temperature UV/vis spectrum of the monomeric gallylene **2** in Et_2O revealed an absorption at λ_{max} at 440 nm (ε = 2081 mol L^{-1} cm^{-1}) (Fig. S55†). In comparison to digallene **1**, the absorption is blue shifted and less intense (for **1**: λ_{max} = 501 nm (ε = 9847 mol L^{-1} cm^{-1})). The shorter wavelength absorption and the weaker extinction coefficient observed for **2** are both consistent with the n → p transition expected for a gallylene monomer rather than the π to π^* transition observed for digallene **1**.

Visual inspection revealed that upon cooling an Et_2O solution of monomeric gallylene **2** to 223 K, a colour change from yellow to red was observed. A UV/vis spectrum recorded at 223 K reveals a new intense absorption, at $\lambda_{max} = 510$ nm, substantially red-shifted from the one observed at room temperature (Fig. S55†). The low-temperature absorption falls in the region expected for a Ga=Ga π to π^* transition in a *trans*-bent digallene (*cf.* **1**, $\lambda_{max} = 501$ nm).

DFT and TD-DFT calculations support the assignment of the low-temperature 510 nm absorption to a dimer of **2**, the *trans*-bent digallene $[\mathbf{2}]_2$. Using DFT calculations (BP86-D3/Def2SVP) we identified a dimeric structure $[\mathbf{2}]_2$ (Fig. S1†) as a minimum on the potential energy surface located 1.2 kcal mol^{-1} higher than the monomer(s) at 298 K (see later). The geometry calculated for $[\mathbf{2}]_2$ reveals a *trans*-bent Ga=Ga core. A long Ga–Ga distance compared to that determined experimentally for **1** (2.612 Å *vs.* 2.480(1) Å) and much-reduced WBI (0.89 *vs.* 1.24) indicate a significantly weaker bonding interaction for $[\mathbf{2}]_2$ as compared to **1**.

TD-DFT calculations on the optimised structure of $[\mathbf{2}]_2$ predict an absorbance at 569 nm arising from a transition akin to that found for digallene **1**, with substantial Ga=Ga π to π^* character (HOMO → LUMO (Fig. S4†)). At 569 nm the absorption is red shifted by ~60 nm compared to that observed experimentally, but is consistent with the trend between experiment and TD-DFT for digallene **1**.

In benzene or toluene solutions, gallylene **2** appears essentially monomeric; even at lower temperatures, no evidence of dimerisation could be observed using NMR spectroscopy. In Et_2O solution, however, UV/vis spectroscopy revealed the presence of the dimer $[\mathbf{2}]_2$. Gallylene **2** thus occupies the opposite end of a continuum it shares with digallene **1**.

The finely-balanced energetics of the monomer/dimer equilibria of **1** and **2**/$[\mathbf{2}]_2$ (see below) are further emphasised by the observation that gallylene **2** may also be crystallised as an elongated dimer in the solid state. Crystallisation of **2** from toluene (rather than pentane as described above) solution affords dark red-purple crystals of the weakly associated elongated dimer $L^{Mes/Mes}Ga\cdots GaL^{Mes/Mes}$ (Fig. 5) as a toluene solvate.

X-ray crystallography revealed long Ga···Ga interactions between two crystallographically inequivalent gallium(I) centres. The Ga···Ga distance, at 2.8566(4) Å, is almost 0.4 Å longer than that of the amidophosphine digallene **1** and NHC/silyl digallene **II**.[22] It is however comparable to Power's weakly associated gallium(I) dimer **I** in which the Ga···Ga distance is 2.627(1) Å.[24]

In the elongated $L^{Mes/Mes}Ga\cdots GaL^{Mes/Mes}$ dimer, the relative arrangement of amidophosphine ligands about the Ga···Ga interaction reveal considerable *trans*-bending (θ: 78.37°) and twisting (NGaP : NGaP interplanar angle, $\tau = 89.10°$). Ga1 is trigonal pyramidal, whilst Ga2 has an unusual T-shaped geometry, with P2 and Ga1 disposed *trans* to each other (Ga1–Ga2–P2 = 162.23(2)°). The Ga–P distance at T-shaped Ga2 is shorter than at Ga1 (2.6492(7) Å *vs.* 2.7282(8)). Both Ga–P distances are longer than in the dimeric digallene **1** (2.472(2)/2.513(6) Å), but remain comparable to those in monomeric gallylene **2** (2.7093(5) Å).

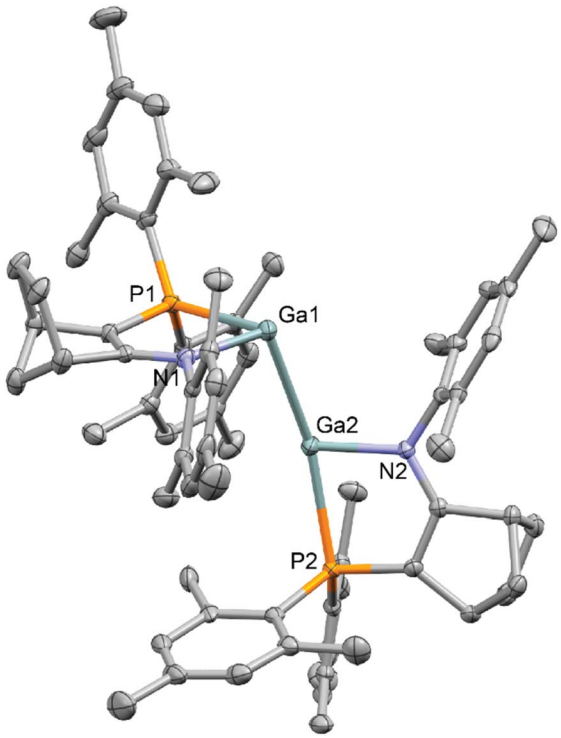

Fig. 5 X-ray structure of $L^{Mes/Mes}Ga\cdots GaL^{Mes/Mes}$ (H atoms omitted for clarity). Thermal ellipsoids at 50% probability. Selected bond distances (Å) and angles (°): Ga1–Ga2 2.8566(4), Ga1–N1 2.040(2), Ga1–P1 2.7282(8), N1–Ga1–P1 78.42(6), Ga2–N2 1.994(2), Ga2–P2 2.6492(7), N2–Ga2–P2 80.23(6).

To evaluate the role of ligand effects on the Ga–Ga bond dissociation energies of digallenes **1** and $[\mathbf{2}]_2$, we calculated dissociation energies for the two dimers using DFT (BP86-D3/def2svp). Dissociation for digallene **1** (bearing $L^{tBu/Mes}$ ligands) was calculated to be thermodynamically unfavourable; $\Delta H = 30.1$, $\Delta G° = 13.9$ kcal mol^{-1}. In contrast $[\mathbf{2}]_2$, with bulkier $L^{Mes/Mes}$ ligands has a thermodynamic preference for the monomeric state; $\Delta H = 17.9$, $\Delta G° = -1.2$ kcal mol^{-1}. These values are consistent with the experimentally observed behaviour of **1** and **2**/$[\mathbf{2}]_2$.

There is a considerable difference in the calculated ΔH for dissociation of **1** and $[\mathbf{2}]_2$ to monomers (30.1 and 17.9 kcal mol^{-1} respectively). An account by Mears and Power highlighted the importance of attractive dispersion interactions in multiply-bonded heavier main-group systems.[37] To estimate their contribution to the stability (or otherwise) of the digallenes **1** and $[\mathbf{2}]_2$, we examined the simple model digallene $[Me_3P(Me_2N)Ga]_2$. By comparing the bond dissociation enthalpies of the full digallene systems with those of the minimal models, we gain insight into stabilising contributions of the larger ligands, which in part will include dispersion. The Ga–Ga bond length in the minimal model was fixed to 2.482 Å or 2.612 Å to represent **1** or $[\mathbf{2}]_2$ respectively. ΔH for dissociation of the minimal models of **1** and $[\mathbf{2}]_2$ proved very similar, at 13.7

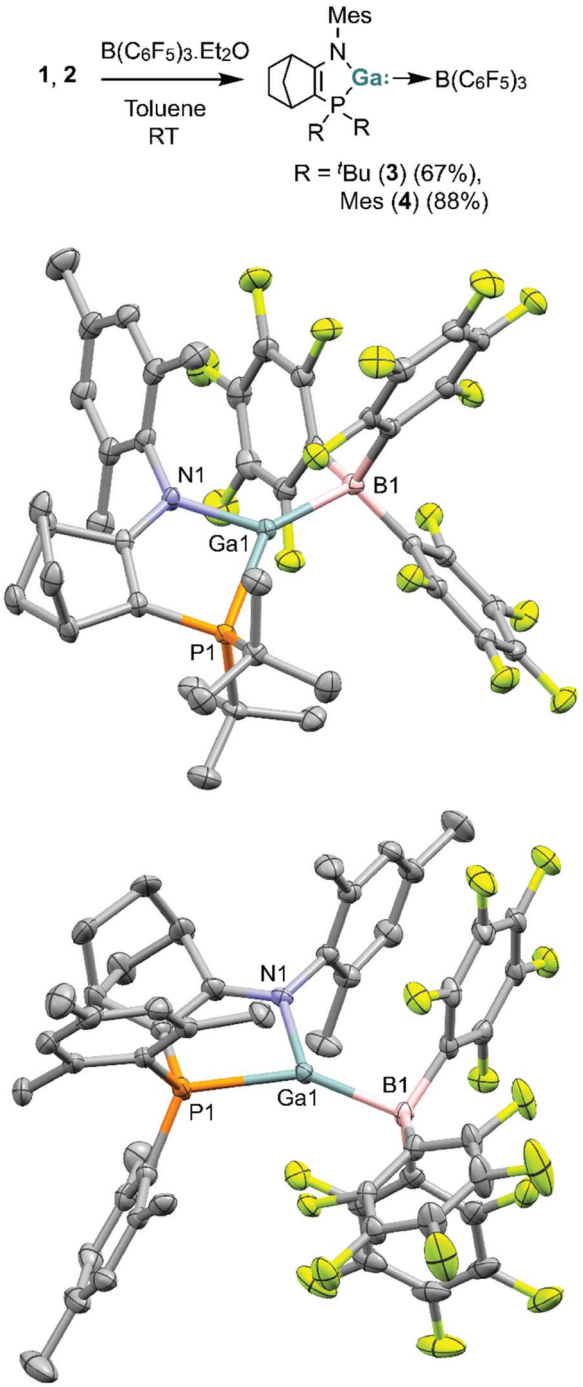

Fig. 6 Synthesis of compounds **3** and **4** (top). X-ray crystal structures of **3** and **4** (H atoms are omitted). Thermal ellipsoids at 50% probability. Selected bond distances (Å) and angles (°) **3**: Ga1–B1 2.121(2), Ga1–N1 1.904(2), Ga1–P1 2.4401(6), N1–Ga1–P1 87.51(5). **4**: Ga1–B1: 2.128(3), Ga1–N1 1.915(2), Ga1–P1 2.4489(7), N1–Ga1–P1 87.38(6).

and 14.7 kcal mol^{-1} respectively, despite the longer Ga–Ga distance in the model for $[\mathbf{2}]_2$. In fact, a relaxed potential energy surface scan of the minimal model revealed that the system is rather insensitive to extension of the Ga–Ga distance, with the energy varying by <1 kcal mol^{-1} over the range 2.48–3 Å (Fig. S3†). The contribution of the ligand ($L^{Mes/tBu}$ *vs.* $L^{Mes/Mes}$) to the stability of the Ga dimers is much more substantial than the Ga–Ga distance. For $[\mathbf{2}]_2$ and its model, there was minimal difference in ΔH for dissociation (14.7 *vs.* 17.9 kcal mol^{-1}), in contrast to the comparison between **1** and its model (13.7 *vs.* 30.1 kcal mol^{-1}). We conclude that digallene **1** is, to a large degree, stabilised by attractive dispersion interactions between the $L^{tBu/Mes}$ ligands that are absent in the digallene $[\mathbf{2}]_2$ bearing the much bulkier $L^{Mes/Mes}$ ligand.

Reactions of 1 and 2 with $B(C_6F_5)_3$

Having established that accessible gallylene–digallene equilibria existed (from opposite sides) in solution for **1** and **2**, we sought to investigate the implications of these equilibria on reactivity.

Treatment of **1** or **2** with tris(pentafluorophenyl)borane, $B(C_6F_5)_3$, proceeded with immediate colour changes to pale yellow. The respective Lewis adducts ($L^{Mes/R}$)Ga–$B(C_6F_5)_3$ (**3**, R = ^{t}Bu, **4**, R = Mes) were isolated in high yields as pale-yellow crystalline solids after work-up (Fig. 6).

Formation of compounds **3** and **4** was confirmed by NMR spectroscopy. $^{31}P\{^1H\}$ NMR spectra of **3** and **4** revealed resonances at δ_P 15.3 and −47.2, respectively. The ^{11}B NMR spectra of **3** and **4** showed singlets at δ_B −19.0 and −18.2, respectively, shifted upfield from free $B(C_6F_5)_3$ (δ 58.0).

The single crystal X-ray structures of **3** and **4** confirmed coordination of Ga to B, with Ga–B distances (**3**, 2.121(2) Å; **4**, 2.128(3) Å) consistent with previously reported Ga–$B(C_6F_5)_3$ dative interactions (range 2.108(1)–2.185(2) Å).[15,38] Notably, the Ga(1)–P(1) distance in **4** is substantially contracted – by 0.26 Å – compared to in the free monomer **2**. This is consistent with the observed upfield shift of 9.4 ppm in the ^{31}P NMR upon coordination of $B(C_6F_5)_3$.

Whilst the formation of the gallylene adduct **4** is expected, the analogous adduct **3** arising from the digallene **1** and $B(C_6F_5)_3$ is additional evidence that the corresponding monomer is energetically accessible in solution.

Reactions of 1 and 2 with an oxidant

Tan, Wang and coworkers reported that the NHC-coordinated digallene **II** can be singly or doubly oxidised by treatment with an appropriate amount of $[Ph_3C][B(3,5\text{-}(CF_3)_2C_6H_3)_4]$.[22] We were curious to know whether compounds **1** and **2** could be oxidised in similar fashion.

The reaction of digallene **1** with two equivalents of $[Ph_3C][B(C_6F_5)_4]$ in fluorobenzene at room temperature initially formed a brown solution, which quickly turned green. Within minutes, crystalline dark green needles precipitated from the solution. X-ray crystallography revealed the product of the reaction to be $[^{Mes/tBu}LGa\text{-}GaL^{Mes/tBu}]^{2+}$ (**5**), the result of a 2-electron oxidation of **1**. The dication **5** crystallised as the fluorobenzene solvate $[^{Mes/tBu}LGa\text{-}GaL^{Mes/tBu}][B(C_6F_5)_4]_2\cdot 2(C_6H_5F)$ (Fig. 7).

The double oxidation of digallene **1** to form the dication **5** induces substantial structural changes around the Ga_2 unit, which in **5** adopts a planar conformation in contrast to the *trans*-bent Ga=Ga unit of **1**. Ga1 and Ga1′ deviate from the N1,

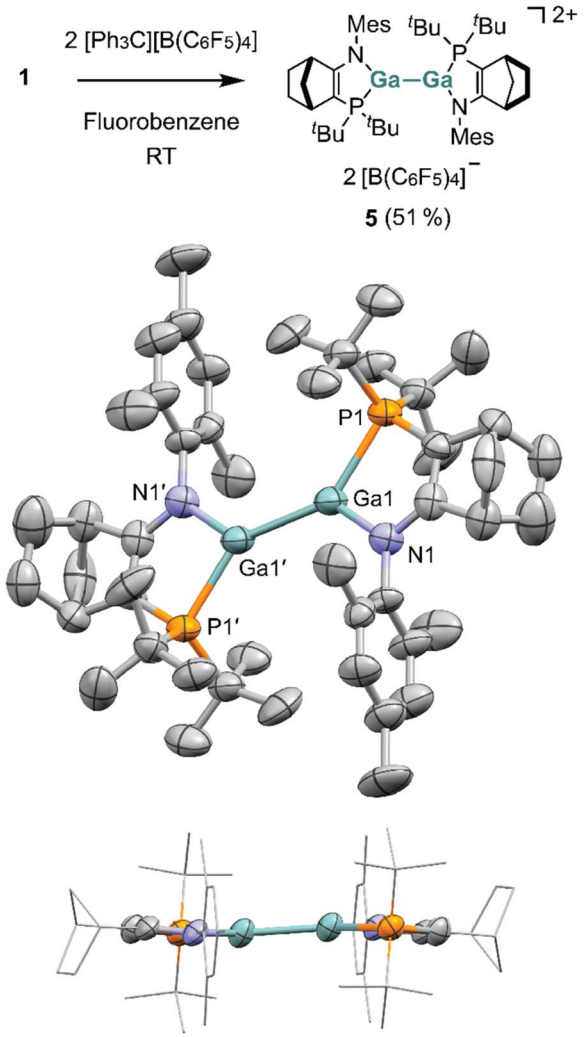

Fig. 7 Synthesis of $[^{Mes/tBu}LGa\text{-}GaL^{Mes/tBu}][B(C_6F_5)_4]_2$ (top). X-ray structure of **5** from crystals of $[^{Mes/tBu}LGa\text{-}GaL^{Mes/tBu}][B(C_6F_5)_4]_2\cdot 2(C_6H_5F)$ (H atoms, $[B(C_6F_5)_4]^-$ counter anions and PhF molecules omitted for clarity). Thermal ellipsoids at 50%. Bond distances: **5**: Ga–Ga 2.390(2) Å.

P1, N1′,P1′ plane by just 0.05 Å. This is in contrast to the dication of digallene **II**, $[\mathbf{II}]^{2+}$ reported by Wang and Tan, which is twisted with a dihedral angle of 73.77°.[22] The Ga–Ga bond length in dication **5** is 2.390(2) Å, which is shorter than that in the corresponding digallene **1** (2.480(1) Å). DFT calculations on dication **5** (BP86/Def2SVP) return an optimised structure with a Ga–Ga distance (2.398 Å) that closely replicates that determined experimentally. NBO calculations reveal the Wiberg bond index of the Ga–Ga bond in **5** is 0.90, (*vs.* 1.02 for $[\mathbf{II}]^{2+}$), consistent with a single bond. The Ga–Ga σ bonding orbital is found at −11.771 eV as HOMO−6. The contraction of the Ga–Ga distance in **1** upon oxidation (*vs.* the lengthening observed for **II**) is largely consequence of the highly *trans*-bent structure adopted by **1**.

Subsequent preparations of **5** resulted in crystallisation of the dication as a different solvate, $[^{Mes/tBu}LGa\text{-}GaL^{Mes/tBu}][B(C_6F_5)_4]_2\cdot 4(C_6H_5F)$. Notably, these crystals were blue rather than green. Close inspection of the structures (see Table S8†) revealed no significant differences in geometry around the central Ga_2 unit and N,P ligand. Neither structure displays close Ga–F interactions with fluorobenzene or $[B(C_6F_5)_4]^-$ anion, with the closest "contact" in either being 4.673 Å (sum of Ga + F VdW radii = 3.34 Å). However, in both structures the shortest Ga–F distances are located directly above/below the plane of the Ga_2 unit. The two structures differ in the number of F atoms distributed around that plane, with four present in the $\cdot 2(C_6H_5F)$ solvate and two in the $\cdot 4(C_6H_5F)$ solvate (Fig. S57†). These differing patterns of Ga–F may serve to explain the difference in colour.

The intense green/blue colour of the dication **5** in PhF solution or as crystalline solvates is surprising, given that $[\mathbf{II}]^{2+}$ is colourless. The extremely low solubility of **5** precluded UV/vis spectroscopic studies. We turned to TD-DFT calculations to understand the electronic structure of **5**.

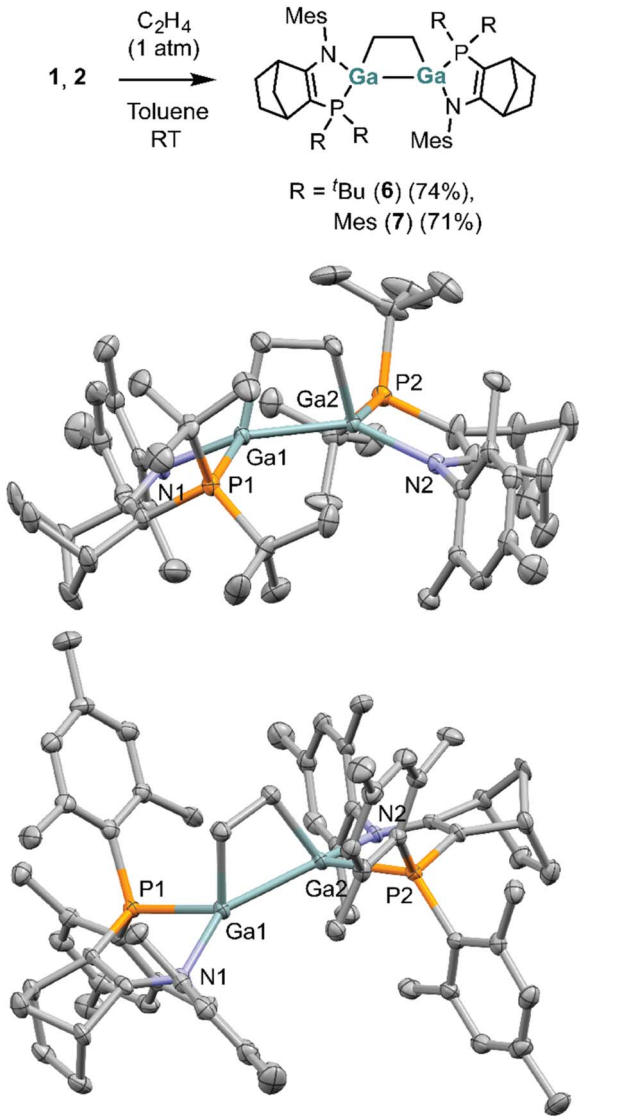

Fig. 8 Synthesis of compounds **6** and **7** (top). X-ray structures of compounds **6** and **7** (H atoms omitted for clarity). Thermal ellipsoids at 50%. **6**: Ga–Ga 2.4799(7) Å, Ga–C 2.027(4)–2.043(4) Å; **7**: Ga–Ga 2.5011(8) Å, Ga–C 2.023(5)–2.031(5) Å.

The LUMO of **5** has Ga–Ga π-bonding character and, at −8.824 eV, is low-lying; its HOMO is essentially ligand based and has C=C π-bonding and N-lone pair character. HOMO−1 has delocalised N–Ga–Ga–N π-bonding character (Fig. S58†). In the UV-vis spectrum predicted by TD-DFT (Fig. S56†) the most intense absorption, at 784 nm, arises from a HOMO → LUMO transition. Such a low-energy transition is not observed in the colourless NHC-coordinated dication $[\mathbf{II}]^{2+}$ because its twisted structure raises the energy of Ga–Ga π-bonding LUMO.

When we treated the monomeric gallylene **2** with $[Ph_3C][B(C_6F_5)_4]$ (0.5 or 1 equiv.) we observed colour changes to red, brown or green, but to date we have been unable to isolate or characterise any gallium-containing products from this reaction. Similarly, when attempting the 1-electron oxidations of **1** or **2** to prepare the radical cation, or attempting comproportion-based routes from **5** and **1**, we have also been unable to obtain isolable products.

Reversible reactions with ethene

Having shown that the digallene **1** can react as a monomer (as well as the already-predominantly-monomeric gallylene **2**), we wanted to investigate the reactivity of **1** and **2** with ethene, considering previously reported Ga(I)/alkene chemistry[17,25] and the reaction of dialumenes with ethene to form dialuminacyclobutanes.[19]

Treatment of toluene solutions of **1** or **2** with ethene (1 atm) at ambient temperature resulted in immediate formation of the 1,2-digallacyclobutanes, **5** and **6** respectively, as apparent [2 + 2] cycloaddition products. The isolation of the 1,2-digallacyclobutane products is in contrast with previous experiments that revealed bis(terphenyl)digallenes react with 2 equivalents of ethene to form 1,4-digallacyclohexanes.[15] Even after heating **1** or **2** to 80 °C under 1 atm ethene for 3 days, we did not observe further incorporation of ethene. Slow cooling of concentrated toluene solutions of **6** or **7** allowed for formation of crystals suitable for analysis *via* single crystal X-ray diffraction (Fig. 8). In both solid-state structures, the phosphorus donors are orientated *anti* across the Ga–Ga bonds, suggesting that the products may arise from reactions of ethene with *E* isomers of the digallene **1** or $[\mathbf{2}]_2$. Ga–Ga and Ga–C bond distances in the metallacycles are consistent with single bonds (**6**: Ga–Ga 2.4799(7) Å, Ga–C 2.027(4)–2.043(4) Å; **7**: Ga–Ga 2.5011(8) Å, Ga–C 2.023(5)–2.031(5) Å). C–C bond distances are also consistent with single bonds (1.533(6) Å in **6**, 1.555(6) Å in **7**. Narrow Ga–Ga–C and C–C–Ga angles give rise to distorted Ga_2C_2 rings with significant out-of-plane twisting (sum of internal angles: **6**, 348.1°, **7**, 354.3°).

As in the digallenes **1** and $[\mathbf{2}]_2$, the gallium atoms in digallacyclobutanes **6** and **7** are stereogenic. In the structure of **6**, the disordered positions of carbon atoms of the norbornene bridge thus indicate that **6** crystallises as a mixture of 3 diastereomers

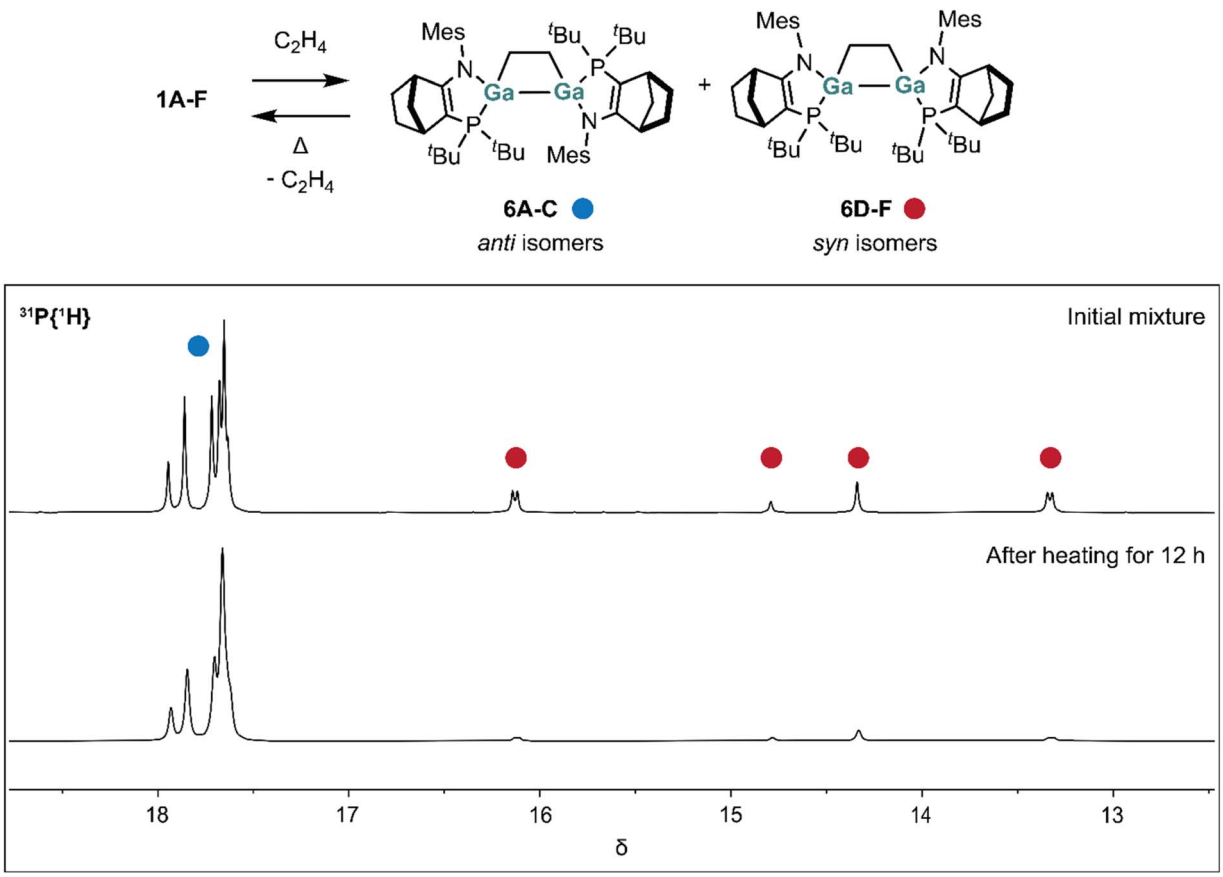

Fig. 9 Reversible ethene binding to **1** (top). $^{31}P\{^1H\}$ NMR spectra showing thermally induced conversion of *syn* isomers **6D–F** to *anti* isomers **6A–C**.

(corresponding to digallene diastereomers **1A**, **1B** and **1C** (Fig. S56†)). That mixture would be expected to give rise to four signals in the ^{31}P NMR spectrum, which we indeed observed in C_6D_6 solutions prepared from crystalline **6** (**6A**/**6B** δ 17.9, 17.6 (both d, $^3J_{PP} = 17$ Hz; **6C** δ 17.6(s), 17.7(s)).

When we exposed digallene **1** in C_6D_6 to 1 atm of ethene and immediately acquired $^{31}P\{^1H\}$ NMR spectra, besides the four resonances assigned to **6A–C**, we observed four additional signals at δ 16.1 (d, $^3J_{PP} = 5$ Hz), 14.8 (s), 14.3 (s), 13.3 (d, $^3J_{PP} = 5$ Hz). We assign these signals to the diastereomers **6D–F**, in which the phosphorus centres are *syn* across the Ga–Ga bonds. Consistent with the much different P–Ga–Ga–P torsion angles in **6C** and **6F**, we note the reduced size of $^3J_{PP}$ in the latter (5 Hz *vs.* 17 Hz).

In the initial (kinetically determined) product mixture formed from **1** and ethene the *anti* (**6A–C**) and *syn* (**6D–F**) isomers are present in a ratio of ~4 : 1. This ratio is determined by a combination of the equilibrium concentrations of the digallene diastereomers (which likely includes, although not observed in our variable temperature NMR studies on **1**, *Z* digallene isomers **1D–F**), the barriers to interconversion of **1A–F**, and those to ethene addition.

On heating the mixture to 80 °C for 12 hours, the *syn* isomers **6D–F** are converted to the thermodynamically preferred *anti* isomers **6A–C**, resulting in an *anti*:*syn* ratio of ~12 : 1 (Fig. 9).

In contrast to **1**, when digallene **2**/$[\mathbf{2}]_2$ is treated with 1 atm ethene, $^{31}P\{^1H\}$ NMR spectroscopy revealed just one major

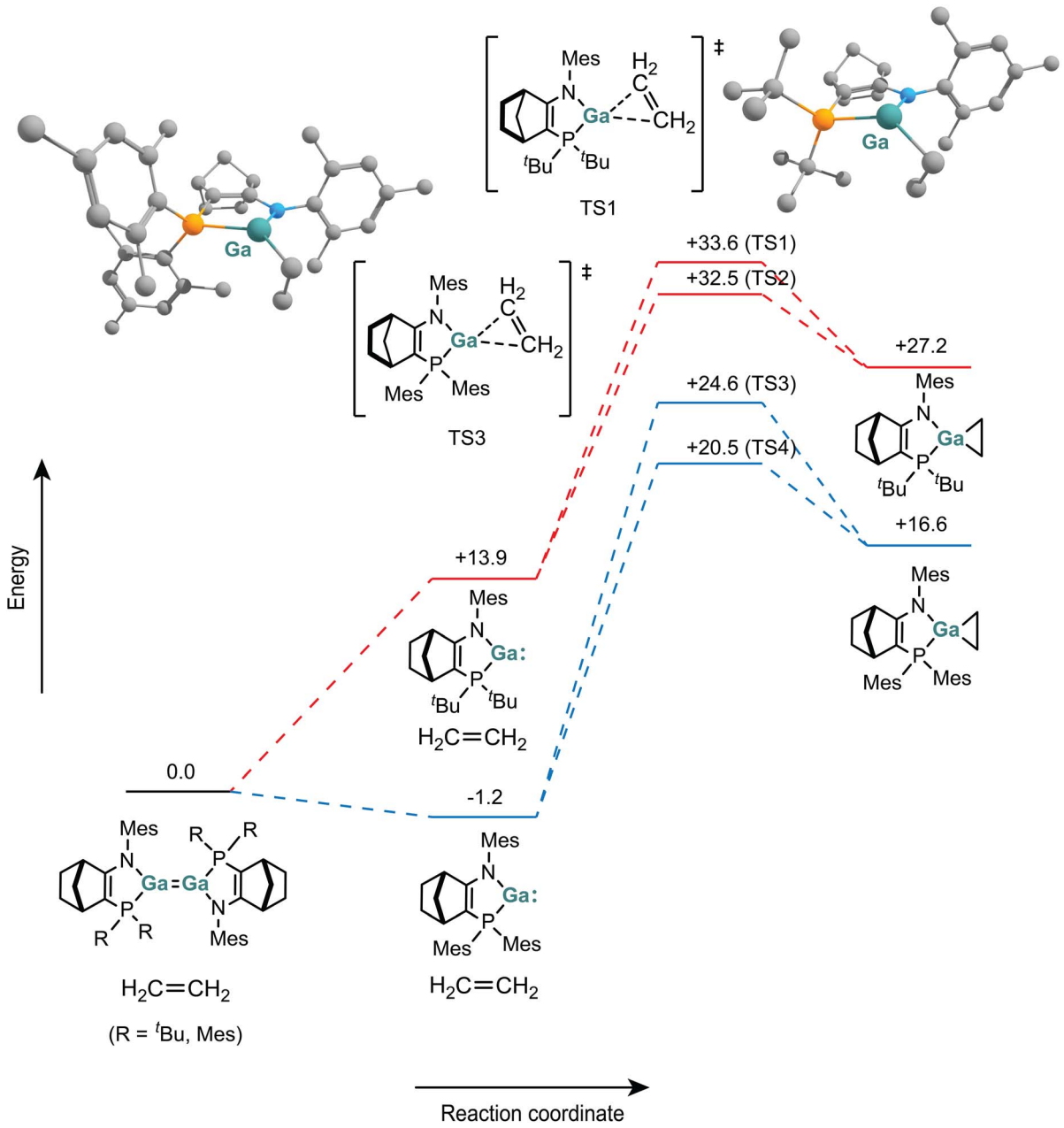

Fig. 10 Calculated reaction pathways for the addition of ethene to monomers (energies in kcal mol^{-1}). Transition states TS2 and TS4 are included in the ESI.†

diastereomer of digallacyclobutane **7** in the initial product mixture (δ −40.0, s). This is consistent with the solid-state structure of **6** which contains a single diastereomer.

For digallacyclobutane **6**, the thermally induced conversion of *syn*-isomers **6D–5F** to the more stable *anti*-isomers **6A–5C** suggests the possibility of reversibility in the formation of **6** (and potentially the $L^{Mes/Mes}$ system **7**). Indeed, when toluene solutions of analytically pure samples of **6** or **7** were heated to 80 °C under an argon atmosphere, the dissociation of ethene was observed (Fig. S49 and S50†). On cooling to room temperature, rapid recombination of **1** and ethene resulted in formation of a mixture of *anti*- and *syn*-isomers (~12 : 1 ratio). The same regeneration of the digallacyclobutane product was observed when previously heated samples of **7** were returned to room temperature.

Further demonstrating the ready reversibility of ethene addition to digallenes **1** and $[\mathbf{2}]_2$, the addition of $B(C_6F_5)_3 \cdot Et_2O$ to isolated samples of **6** and **7** resulted in the complete dissociation of ethene and formation of the Lewis adducts **3** and **4**, respectively.

Likely mechanism of reactions with ethene

We investigated the reactions of **1** and $[\mathbf{2}]_2$ with ethene using DFT methods (BP86/Def2SVP) (Fig. 10). Two obvious mechanisms exist for the formation of digallcyclobutanes: (i) a direct "[2 + 2]" cycloaddition of ethene to digallene, or (ii) [1 + 2] cycloaddition of ethene with gallylene monomer to form a gallacyclopropane intermediate, which then undergoes a C–Ga insertion reaction with a second gallylene monomer.

For reaction of ethene with monomeric gallylene, **1** must first dissociate to the monomer $\mathbf{1_M}$, which lies 13.9 kcal above the digallene. In the $L^{Mes/Mes}$ system, the monomer **2** is lower in energy than digallene $[\mathbf{2}]_2$ anyway (and thus the major species in solution). For both digallene **1** and gallylene **2**, the formation of the gallacyclopropane products was calculated to be substantially endergonic (+27.2 kcal mol^{-1} and +17.8 kcal mol^{-1} respectively).

We were able to locate transition states for the addition of ethene to gallylene $\mathbf{1_M}$ and **2**. The CH_2 and CH_2CH_2 bridges of the norbornenyl ligand backbone mean that the approach of ethene from either "face" of the ligand are energetically differentiated, which leads to two transition states for each gallylene monomer. For the $L^{Mes/Mes}$ gallylene **2**, barriers to ethene addition are +21.7 and 25.8 kcal mol^{-1}. Approach from the CH_2CH_2 "face" has the higher barrier. The same pattern is found for addition to gallylene $\mathbf{1_M}$, with barriers of +18.6 and +19.7 kcal mol^{-1}.

Combined with the energetic cost of monomerisation, the complete barriers for the reaction of digallene **1** with ethene to form the gallacyclopropane are +32.5/33.6 kcal mol^{-1}. Such barriers would be incompatible with the observed reaction rates (within seconds at room temperature), making formation of digallacyclobutanes **6** and **7** *via* initial [1 + 2] addition unlikely.

By DFT, ΔG^0 for formation of the experimentally observed digallacyclobutane products **6** and **7** ($\Delta G^0 = -9.1$ kcal mol^{-1} and −27.0 kcal mol^{-1} respectively) is substantially more favourable than that calculated for formation of the gallacyclopropanes. Unfortunately, despite substantial effort, we were unable to locate transition states for direction addition of ethene to the digallenes **1** or $[\mathbf{2}]_2$ using DFT methods. Our failure to locate such transition states may be due to radical reaction pathways. For both dialumenes and digallenes, DFT methods have been found to imperfectly represent electronic and geometric structures because of substantial diradical character.[39,40] In the closely-related disilenes ($R_2Si = SiR_2$), which themselves have some diradical character, addition of alkynes or other unsaturated compounds to form disilacyclobutenes (or similar) is known to proceed stepwise through radical intermediates.[41,42]

We suggest that the mechanism of the reaction of ethene with digallene **1** and gallylene **2** may proceed *via* a radical pathway involving addition to the digallenes **1** or $[\mathbf{2}]_2$ (akin to disilenes) (particularly considering the mismatch between experimentally observed rates of reaction and the calculated barriers for the reactions of ethene with the monomeric gallylenes). We are currently undertaking a more detailed experimental and computational study of the mechanism of these reactions.

Conclusions

We have demonstrated straightforward synthetic access to amidophosphine-supported gallium(I) systems. Digallene **1** is a *trans*-bent dimer in the solid-state, reversibility dissociating to monomer in solution. Gallylene **2** crystallises as a monomer or weakly associated dimer, but in solution can dimerise to form the digallene $[\mathbf{2}]_2$.

Compounds **1** and **2** demonstrate dual functionality by displaying reactivity consistent with both monomeric gallylenes or dimeric digallenes in solution. The accessibility of monomeric species $\mathbf{1^M}$ and **2** is demonstrated by their reactivity with tris(-pentafluorophenyl)borane, forming the gallylene adducts **3** and **4**. By contrast, the reactions of **1** and **2** with ethene proceed through apparent [2 + 2] cycloaddition reactions, demonstrating that these species can also react (at least formally) as digallenes. Furthermore, the latter reactions are reversible, reforming free ethene and regenerating the Ga(I) species **1** and **2** at elevated temperatures.

The reversible activation of ethene by metal–metal multiply-bonded compounds has been observed in digermynes and distannynes,[13,43] but the reversible reactions of **1** and **2** with ethene are the first unequivocal example of such reactivity of homometallic group 13 multiple bonds. Reversible cycloadditions with alkenes and alkynes have also been observed for monomeric Al(I) species,[14] whilst polyolefins have been observed to react reversibly with terphenyl Ga(I) systems.[17] Reversibility of the type shown by these compounds, and gallium systems **1** and **2**, is a probable prerequisite for the development of transition-metal-like catalysis at main-group centres. Another component towards realising such a goal will be the ability to control reactivity at the main-group centre. Here, we have also shown how variation in the electronic and steric properties of the donor ligand can shift the equilibrium between predominantly dimeric (**1**) or monomeric (**2**) systems.

Data availability

The data supporting this article have been included as part of the ESI.† Crystallographic data has been deposited at the CCDC under CCDC records 2384332–2384338, 2433601, and 2433602, and can be obtained from **https://www.ccdc.cam.ac.uk/structures/**

Author contributions

RJS and MJC proposed and initiated the study. Synthetic work and experimental characterisation was conducted by RJS and MAB. DFT calculations were carried out by RJS and MAB. GSN performed crystallography. RJS, MAB, and MJC co-wrote the manuscript. All authors discussed and commented on the manuscript.

Conflicts of interest

There are no conflicts to declare.

Acknowledgements

This work received funding from the Leverhulme Trust in the form of a Research Project Grant, and from the European Research Council (ERC) under the EU Horizon 2020 research and innovation programme (ERC-2016-STG-716315).

Notes and references

1 T. Chu and G. I. Nikonov, *Chem. Rev.*, 2018, **118**, 3608–3680.
2 P. P. Power, *Nature*, 2010, **463**, 171–177.
3 J. M. Lipshultz, G. Li and A. T. Radosevich, *J. Am. Chem. Soc.*, 2021, **143**, 1699–1721.
4 H. W. Moon and J. Cornella, *ACS Catal.*, 2022, **12**, 1382–1393.
5 S. Bonfante, C. Lorber, J. M. Lynam, A. Simonneau and J. M. Slattery, *J. Am. Chem. Soc.*, 2024, **146**, 2005–2014.
6 H. Fujimoto, T. Kodama, M. Yamanaka and M. Tobisu, *J. Am. Chem. Soc.*, 2020, **142**, 17323–17328.
7 C. Weetman and S. Inoue, *ChemCatChem*, 2018, **10**, 4213–4228.
8 D. J. D. Young and R. West, *Chem. Lett.*, 1986, **15**, 883–884.
9 C. Cui, M. M. Olmstead and P. P. Power, *J. Am. Chem. Soc.*, 2004, **126**, 5062–5063.
10 R. Kinjo, M. Ichinohe, A. Sekiguchi, N. Takagi, M. Sumimoto and S. Nagase, *J. Am. Chem. Soc.*, 2007, **129**, 7766–7767.
11 R. Rodriguez, D. Gau, T. Kato, N. Saffon-Merceron, A. De Cózar, F. P. Cossío and A. Baceiredo, *Angew. Chem., Int. Ed.*, 2011, **50**, 10414–10416.
12 Y. Peng, B. D. Ellis, X. Wang, J. C. Fettinger and P. P. Power, *Science*, 2009, **325**, 1668–1670.
13 T. Sugahara, J.-D. Guo, T. Sasamori, S. Nagase and N. Tokitoh, *Chem. Commun.*, 2018, **54**, 519–522.
14 C. Bakewell, A. J. P. White and M. R. Crimmin, *Chem. Sci.*, 2019, **10**, 2452–2458.
15 N. J. Hardman, R. J. Wright, A. D. Phillips and P. P. Power, *J. Am. Chem. Soc.*, 2003, **125**, 2667–2679.
16 Z. Zhu, R. C. Fischer, B. D. Ellis, E. Rivard, W. A. Merrill, M. M. Olmstead, P. P. Power, J. D. Guo, S. Nagase and L. Pu, *Chem.–Eur. J.*, 2009, **15**, 5263–5272.
17 C. A. Caputo, J.-D. Guo, S. Nagase, J. C. Fettinger and P. P. Power, *J. Am. Chem. Soc.*, 2012, **134**, 7155–7164.
18 P. Dabringhaus, H. Scherer and I. Krossing, *Nat. Synth.*, 2024, **3**, 732–743.
19 R. L. Falconer, K. M. Byrne, G. S. Nichol, T. Krämer and M. J. Cowley, *Angew. Chem., Int. Ed.*, 2021, **60**, 24702–24708.
20 P. Bag, A. Porzelt, P. J. Altmann and S. Inoue, *J. Am. Chem. Soc.*, 2017, **139**, 14384–14387.
21 C. Weetman, A. Porzelt, P. Bag, F. Hanusch and S. Inoue, *Chem. Sci.*, 2020, **11**, 4817–4827.
22 Z. Feng, Y. Fang, H. Ruan, Y. Zhao, G. Tan and X. Wang, *Angew. Chem., Int. Ed.*, 2020, **59**, 6769–6774.
23 N. J. Hardman, B. E. Eichler and P. P. Power, *Chem. Commun.*, 2000, 1991–1992.
24 N. J. Hardman, R. J. Wright, A. D. Phillips and P. P. Power, *Angew. Chem., Int. Ed.*, 2002, **41**, 2842–2844.
25 C. A. Caputo, Z. Zhu, Z. D. Brown, J. C. Fettinger and P. P. Power, *Chem. Commun.*, 2011, **47**, 7506.
26 C. Dohmeier, D. Loos and H. Schnöckel, *Angew Chem. Int. Ed. Engl.*, 1996, **35**, 129–149.
27 A. L. Hawley, C. A. Ohlin, L. Fohlmeister and A. Stasch, *Chem.–Eur. J.*, 2017, **23**, 447–455.
28 A. Lehmann, J. D. Queen, C. J. Roberts, K. Rissanen, H. M. Tuononen and P. P. Power, *Angew. Chem.*, 2024, e202412599.
29 W. Uhl, U. Schütz, W. Kaim and E. Waldhör, *J. Organomet. Chem.*, 1995, **501**, 79–85.
30 X. He, R. A. Bartlett, M. M. Olmstead, K. Ruhlandt-Senge, B. E. Sturgeon and P. P. Power, *Angew Chem. Int. Ed. Engl.*, 1993, **32**, 717–719.
31 J. Su, X.-W. Li, R. C. Crittendon and G. H. Robinson, *J. Am. Chem. Soc.*, 1997, **119**, 5471–5472.
32 A. Barthélemy, H. Scherer, M. Daub, A. Bugnet and I. Krossing, *Angew. Chem., Int. Ed.*, 2023, **62**(47), e202311648.
33 A. Barthélemy and I. Krossing, *Inorg. Chem.*, 2024, **64**(46), 21763–21787.
34 O. Kysliak, H. Görls and R. Kretschmer, *Dalton Trans.*, 2020, **49**, 6377–6383.
35 D. Sarkar, P. Vasko, A. F. Roper, A. E. Crumpton, M. M. D. Roy, L. P. Griffin, C. Bogle and S. Aldridge, *J. Am. Chem. Soc.*, 2024, **146**, 11792–11800.
36 R. H. Crabtree, *The organometallic chemistry of the transition metals*, Wiley, Hoboken, N.J, 5th edn, 2009.
37 K. L. Mears and P. P. Power, *Acc. Chem. Res.*, 2022, **55**, 1337–1348.
38 N. J. Hardman, P. P. Power, J. D. Gorden, C. L. B. Macdonald and A. H. Cowley, *Chem. Commun.*, 2001, 1866–1867.
39 K. M. Byrne, R. Bjornsson and T. Krämer, *Phys. Chem. Chem. Phys.*, 2024, **26**, 30018–30034.

40 J. Moilanen, P. P. Power and H. M. Tuononen, *Inorg. Chem.*, 2010, **49**, 10992–11000.
41 A. T. Henry, J. L. Bourque, I. Vacirca, D. Scheschkewitz and K. M. Baines, *Organometallics*, 2019, **38**, 1622–1626.
42 K. K. Milnes, L. C. Pavelka and K. M. Baines, *Chem. Soc. Rev.*, 2016, **45**, 1019–1035.
43 S. Wang, T. J. Sherbow, L. A. Berben and P. P. Power, *J. Am. Chem. Soc.*, 2018, **140**, 590–593.